International Journal of Pharmaceutics 434 (2012) 257–263

Contents lists available at SciVerse ScienceDirect

International Journal of Pharmaceutics

journal homepage: www.elsevier.com/locate/ijpharm

Pharmaceutical Nanotechnology

Multifunctional poly (lactide-*co*-glycolide) nanoparticles for luminescence/magnetic resonance imaging and photodynamic therapy

Dong Jin Lee[a], Ga Young Park[b], Kyung Taek Oh[b], Nam Muk Oh[a], Dong Sup Kwag[a], Yu Seok Youn[c], Young Taik Oh[d,*], Jin woo park[e], Eun Seong Lee[a,*]

[a] *Division of Biotechnology, The Catholic University of Korea, 43-1 Yeokgok 2-dong, Wonmi-gu, Bucheon-si, Gyeonggi-do 420-743, Republic of Korea*
[b] *College of Pharmacy, Chung-Ang University, 221 Heukseok dong, Dongjak-gu, Seoul 155-756, Republic of Korea*
[c] *College of Pharmacy, Sungkyunkwan University, 300 Chonchon-dong, Jangan-gu, Suwon-si, Gyeonggi-do 440-746, Republic of Korea*
[d] *Department of Diagnostic Radiology, Yonsei University College of Medicine, 134 Shinchon-dong, Seodaemun-gu, Seoul 120-752, Republic of Korea*
[e] *Amore-pacific Corporation R & D center, 314-1, Bora-dong, Yongin 446-1729, Republic of Korea*

ARTICLE INFO

Article history:
Received 17 April 2012
Received in revised form 17 May 2012
Accepted 26 May 2012
Available online 2 June 2012

Keywords:
Poly (lactide-*co*-glycolide)
Fe_3O_4
Photodynamic therapy (PDT)
Magnetic resonance imaging (MRI)

ABSTRACT

Poly (lactide-*co*-glycolide) (PLGA) coupled with methoxy poly (ethylene glycol) (mPEG) or chlorin e6 (Ce6) was synthesized using the Steglich esterification method. PLGA-linked mPEG (PLGA-mPEG), PLGA-linked Ce6 (PLGA-Ce6), and Fe_3O_4 were utilized to constitute multifunctional PLGA nanoparticles (~160 nm) *via* the multi-emulsion $W_1/O/W_2$ (water-in-oil-in-water) method. The photo-sensitizing properties of Ce6 molecules anchored to PLGA nanoparticles enabled *in vivo* luminescence imaging and photodynamic therapy for the tumor site. The encapsulation of Fe_3O_4 allowed high contrast magnetic resonance (MR) imaging of the tumor *in vivo*. Overall, PLGA nanoparticles resulted in a significant tumor volume regression for the light-illuminated KB tumor *in vivo* and enhanced the contrast at the tumor region, compared to that of Feridex® (commercial contrast agent).

1. Introduction

Colloidal polymeric nanoparticles have the potential to dramatically improve the diagnosis and treatment of tumor (Alivisatos, 2003; Niemeyer, 2001; Ferrari, 2005; Peer et al., 2007; Qian et al., 2008). The ability to fine-tune the properties of nanoparticles by controlling their components in the core or the shell region renders them useful and optimized for pharmaceutical purposes (Alivisatos, 2003; Niemeyer, 2001; Ferrari, 2005; Peer et al., 2007). In the recent years, an increasing number of researchers have assessed the possibility of using nanoparticles for multimodal diagnosis and treatment of tumor cells (Kim et al., 2008; Bagalkot et al., 2007; Piao et al., 2008). These trials have emerged as attractive preference in tumor therapy, as the nanoparticles allow precise detection and monitoring of tumors as well as deliver antitumor drugs to tumors (Kim et al., 2008; Piao et al., 2008). Various examples involve the exploitation of tumor-targeting nanoparticles consisting of lipids, polysaccharides, poly(L-amino acid)s, synthetic amphiphilic polymers, and inorganic particles (Bagalkot et al., 2007; Reddy et al., 2006; Liong et al., 2008). However, even in the case of the well-designed multimodal nanocarriers for diagnosis and therapy, they have been mostly limited to *in vitro* systems with very few successful demonstrations *in vivo* due to the harsh *in vivo* biological conditions and the lack of development of a highly efficient tumor ablation method (Bagalkot et al., 2007; Reddy et al., 2006; Liong et al., 2008).

Poly(D,L-lactide-*co*-glycolide) (PLGA) nanoparticles (Brannon-Peppas and Blanchette, 2004; Lee et al., 2004; Zhang et al., 2007) have been demonstrated as excellent carriers for imaging and targeting of tumor cells and for carrying antitumor drugs to tumor cells, due to their unique features including biocompatibility, biodegradability, tailor-made functionality, and the large interior cargo volume. We newly modified the PLGA nanoparticles using methoxy poly (ethylene glycol) (mPEG) and chlorin e6 (Ce6). mPEG was simply conjugated to PLGA nanoparticles (Fig. 1a) for enhancing the nanoparticle stability in the serum. The conjugation of Ce6 to PLGA nanoparticles was designed to obtain light-driven fluorescent *in vivo* images (Takizawa et al., 2009; Park et al., 2011, 2012; Oh et al., 2012) and to perform photodynamic tumor therapy (Chin et al., 2006; Park et al., 2011, 2012; Oh et al., 2012). It is known that Ce6 is a photoabsorber that exhibits light luminescence (Ochsner, 1997; Hamblin et al., 2001) and generates reactive oxygen species (*e.g.*, singlet oxygen: $^1O_2$) from light absorption (Ochsner, 1997; Hamblin et al., 2001). The released reactive oxygen species lead to irreversibly damage to the treated tumor cells (Park

* Corresponding authors. Tel.: +82 2 2164 4921; fax: +82 2 2164 4865.
E-mail addresses: oytaik@yumc.yonsei.ac.kr (Y.T. Oh), eslee@catholic.ac.kr, hejulu@hanmail.net (E.S. Lee).

0378-5173/$ – see front matter © 2012 Elsevier B.V. All rights reserved.
http://dx.doi.org/10.1016/j.ijpharm.2012.05.068

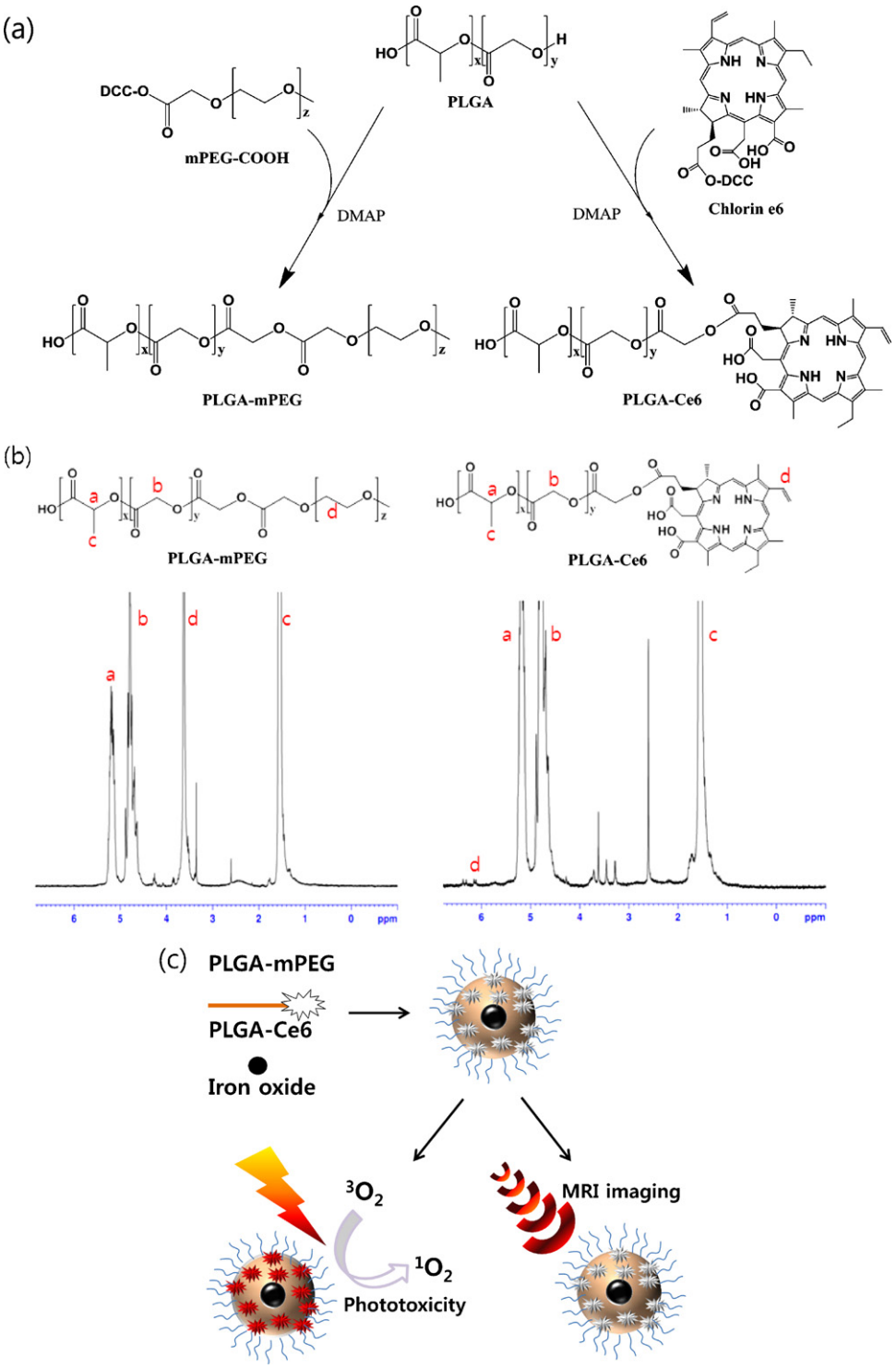

Fig. 1. Preparation of multifunctional PLGA nanoparticles. (a) Synthetic scheme of PLGA-mPEG and PLGA-Ce6. (b) ^{1}H NMR peaks of PLGA-mPEG and PLGA-Ce6. (c) Schematic concept for the multifunctional PLGA nanoparticle. See the text for more details.

et al., 2011, 2012; Oh et al., 2012). These PLGA nanoparticles can also carry inorganic cargo (Fe_3O_4) (Lee et al., 2011b) used for the non-invasive magnetic resonance (MR) imaging of *in vivo* tumors, *via* the multi-emulsion $W_1/O/W_2$ (water-in-oil-in-water) method (Lee et al., 2007). We preferentially examined the multifunctional properties of PLGA nanoparticles with *in vivo* fluorescence techniques, *in vivo* MR imaging experiments, and *in vivo* tumor inhibition tests.

2. Materials and methods

2.1. Materials

Poly(D,L-lactide-*co*-glycolide) (PLGA, RG502H; lactide/glycolide molar ratio = 50/50, M_w = 14 kDa) was provided by Boehringer-Ingelheim (USA). Chlorin e6 (Ce6) was purchased from Frontier Scientific Inc. (USA). Methoxy poly(ethylene glycol) (mPEG,

Table 1
Polymers that constitute the multifunctional PLGA nanoparticles.

Code	Feeding PLGA-Ce6 (wt.%)	Feeding PLGA-mPEG (wt.%)
NP1	75%	25%
NP2	50%	50%
NP3	100%	0%
NP4	0%	100%

M_w = 2 kDa), *N*,*N*′-Dicyclohexylcarbodiimide (DCC), Fe_3O_4, 4-dimethylaminopyridine (DMAP), triethylamine (TEA), pyridine, dichloromethane (DCM), diethyl ether, and dimethyl sulfoxide (DMSO) were purchased from Sigma–Aldrich (USA). RPMI-1640, fetal bovine serum (FBS), penicillin, and streptomycin were purchased from Welgene Inc. (Korea). The Cell Counting Kit-8 was obtained from Dojindo Molecular Technologies Inc. (Japan).

2.2. PLGA-mPEG, PLGA-Ce6 synthesis

PLGA coupled with mPEG (PLGA-mPEG) or Ce6 (PLGA-Ce6) was synthesized using the Steglich esterification method (Neises and Steglich, 1978). Briefly, mPEG (0.2 mM) or Ce6 (0.4 mM) pre-activated with DCC (0.2 mM) was conjugated to the hydroxyl (—OH) group of PLGA (0.1 mM) in DCM (20 mL) including DMAP (0.2 mM), TEA (0.1 mL), and pyridine (0.1 mL) (Fig. 1a). The solution was stirred at room temperature for 1 day. After the reaction, the solution was filtered and lyophilized after adding excess diethyl ether. The resulting product was dissolved in DMSO and transferred to a pre-swollen dialysis membrane tube (Spectra/Por®, MWCO 8K) to remove non-reacted mPEG or Ce6 during the dialysis process. The synthesized polymers were characterized using ^{1}H NMR (Bruker Advance III 400 MHz) and NMR solvent (DMSO-d_6) with TMS.

2.3. PLGA nanoparticle preparation

PLGA nanoparticles were fabricated *via* the multi-emulsion $W_1/O/W_2$ (water-in-oil-in-water) method (Lee et al., 2007). Fe_3O_4 (20 mg) was dispersed in 1 mL of de-ionized water (W_1), PLGA-mPEG and/or PLGA-Ce6 (total 200 mg) (Table 1) was added to 3 mL of DCM solution (O). Two solutions were then mixed together and emulsified (resulting in W_1/O) by vigorous vortexing for 1 min and then injected into 1.0 wt.% PVA and 0.9 wt.% NaCl aqueous solution (W_2). Emulsification ($W_1/O/W_2$) proceeded for 5 min, using a homo-mixer (manufactured by Tokushu Kika Kogyo Corp.) at 12,000 rpm. The solution was then stirred for 1 h to evaporate DCM and was collected after the centrifugation at 20,000 rpm for 20 min. The obtained nanoparticles were subsequently washed three times with PBS pH 7.4 and then freeze-dried for 2 days. Here, Fe_3O_4 concentrations in PLGA nanoparticle were measured using a Jobin-Yvon Ultima-C inductively coupled plasma-atomic emission spectrometer (JY-Ultima-2, France) (Prashant et al., 2010). Before the test, PLGA nanoparticles (10 mg) dissolved in 2 mL of concentrated nitric acid was heated to 110 °C for 45 min and then diluted with deionized water.

2.4. Characterization of PLGA nanoparticles

The particle size distribution of PLGA nanoparticles (0.1 mg/mL) was measured with a Zetasizer 3000 instrument (Malvern Instruments, USA) equipped with a He–Ne Laser beam at a wavelength of 633 nm and a fixed scattering angle of 90°. The morphology of PLGA nanoparticles (10 μg/mL) was confirmed using a field emission scanning electron microscopy (FE-SEM, Hitachi s-4800, Japan). The zeta potential of PLGA nanoparticles (0.1 mg/mL) in phosphate buffer saline (PBS, pH 7.4, 150 mM) was measured using a Zetasizer 3000. The fluorescence image of PLGA nanoparticles (red fluorescence: Ce6) was visualized using a fluorescence microscope (at λ_{ex} 570 nm and λ_{em} 595 nm, E-SCOPE 1500F).

The generation of singlet oxygen of PLGA nanoparticles (equivalent Ce6 10 μg/mL) was confirmed using 9,10-dimethylanthracene (DMA) (Park et al., 2011, 2012; Oh et al., 2012). DMA (20 mmol) was mixed with PLGA nanoparticles (0.01 mg/mL) in PBS (150 mM, pH 7.4). The solution was illuminated at a light intensity of 5.2 mW/cm^2 using a 670 nm laser source for 10 min. When the DMA fluorescence intensity (measured using a Shimadzu RF-5301PC spectrofluorometer at λ_{ex} 360 nm and λ_{em} 380–550 nm) reached a plateau after 1 h, the change in DMA fluorescence intensity (F_f–F_s) was plotted after subtracting each sample fluorescence intensity (F_s) from the full DMA fluorescence intensity (without Ce6, indicating no singlet oxygen, F_f) (Park et al., 2011, 2012; Oh et al., 2012).

2.5. Cell culture

Human nasopharyngeal epidermal carcinoma KB cells were maintained in RPMI-1640 medium with 2 m L-glutamine, 1% penicillin–streptomycin, and 10% FBS in a humidified standard incubator with a 5% CO_2 atmosphere at 37 °C. Prior to testing, cells (1×10^5 cells/mL), grown as a monolayer, were harvested by trypsinization using a 0.25% (w/v) trypsin/0.03% (w/v) EDTA solution. KB cells suspended in RPMI-1640 medium were seeded onto well plates and cultured for 24 h prior to *in vitro* cell testing (Park et al., 2011, 2012; Oh et al., 2012).

2.6. Phototoxicity

Phototoxicity of PLGA nanoparticles with light illumination was tested for KB tumor cells (Park et al., 2011, 2012; Oh et al., 2012). PLGA nanoparticles or free Ce6 dispersed in RPMI-1640 medium were administered to cells plated in 96-well plates. The cells were incubated with each sample for 4 h and then washed three times with PBS (pH 7.4). The cells were illuminated at a light intensity of 5.2 mW/cm^2 using a 670 nm fiber coupled laser system (with continuous wave mode) for 10 min and then further incubated for 6 h in RPMI-1640/FBS medium.

Cell viability was determined using a Cell Counting Kit-8 (CCK-8 assay). In addition, the cell viability test of KB cells treated with PLGA nanoparticles (5–1000 μg/mL) without light illumination for 24 h was conducted to estimate the original toxicity of PLGA nanoparticles.

2.7. Animal care

In vivo studies were conducted with 4 to 6-week old female nude mice (BALB/c, nu/nu mice, Institute of Medical Science, Japan). Mice were maintained under the guidelines of an approved protocol from the Institutional Animal Care and Use Committee (IACUC) of the Catholic University of Korea (Republic of Korea).

2.8. In vivo fluorescence imaging

For the *in vivo* animal experiments, KB tumor cells were introduced into female nude mice *via* subcutaneous injection of 1×10^5 cells suspended in PBS pH 7.4 (ion strength: 0.15) medium. When the tumor volume reached about 80 mm^3, PLGA nanoparticles (*i.v.* dose: equivalent Ce6 0.1 mg/kg) or free Ce6 (*i.v.* dose: 2.5 mg/kg) in PBS (150 mM, pH 7.4) was injected intravenously into the tumor-bearing nude mice through the tail vein. A 12-bit CCD camera (Image Station 4000 MM; Kodak, Rochester, NY, USA) prepared with a special C-mount lens and a long wave emission filter (600–700 nm; Omega Optical, Brattleboro, VT, USA) was used to

capture live fluorescence images of the nude mice (Park et al., 2011, 2012; Oh et al., 2012; Lee et al., 2011a).

2.9. In vivo magnetic resonance (MR) imaging

PLGA nanoparticles (*i.v.* dose: equivalent 0.5 mg Fe/kg) or Feridex® (*i.v.* dose: 5 mg Fe/kg) in PBS (150 mM, pH 7.4) were injected intravenously into the KB tumor-bearing nude mice through the tail vein. All MR imaging experiments were performed with a clinical MR imaging instrument with a micro-47 surface coil (Intera, Philips Medical Systems). For T_2^*-weighted MR imaging of a live nude mice, the following parameters were adopted: point resolution = 156 μm × 156 μm, section thickness = 0.8 mm, TR = 300 ms, TE = 16 ms, number of acquisitions = 3.

2.10. In vivo tumor therapy

PLGA nanoparticles (*i.v.* dose: equivalent Ce6 0.1 mg/kg) or free Ce6 (*i.v.* dose: 2.5 mg/kg) in PBS (150 mM, pH 7.4), or only PBS (150 mM, pH 7.4, as a control) was injected intravenously into the tumor-bearing nude mice through the tail vein. At 24 h after the injection, the tumor sites of the nude mice were locally illuminated for 40 min at a light intensity of 2.8 mW/cm^2 with a 670 nm fiber coupled laser system (with continuous wave mode). The change in tumor volume was monitored over time. Tumor volume was calculated using the formula: tumor volume = length × (width)^2/2.

3. Results and discussion

3.1. Synthesis of PLGA nanoparticles

As shown in Fig. 1a, the terminal hydroxyl (—OH) group of PLGA was coupled to mPEG or Ce6 using DCC and DMAP, assessed by ^{1}H NMR (DMSO-d_6 with TMS) peaks (Fig. 1b). The structure of the core and the shell of PLGA nanoparticles was constructed by the multi-emulsion $W_1/O/W_2$ (water-in-oil-in-water) method. Fe_3O_4 dispersed in de-ionized water (W_1) was emulsified with PLGA-mPEG and/or PLGA-Ce6 in DCM solution (O) and then injected into 1.0 wt.% PVA and 0.9 wt.% NaCl aqueous solution (W_2). This process allowed the fabrication of PLGA nanoparticles consisted of a hydrophilic polymer shell (mPEG) and a hydrophobic core [PLGA, Ce6, Fe_3O_4]. In particular, the photo-sensitizing properties of Ce6 molecules and magnetic-responsive properties of Fe_3O_4 are essential to multifunctional PLGA nanoparticles (Fig. 1c). The PEG blocks on the surface may be effective in minimizing potential immune responses (Kizilel et al., 2010). In addition, we measured the content of Fe_3O_4 encapsulated into PLGA nanoparticles using a Jobin-Yvon Ultima-C inductively coupled plasma-atomic emission spectrometer (Prashant et al., 2010) and found encapsulation of 30–50 mg Fe_3O_4 per 1 g of PLGA nanoparticles.

We prepared various combinations of PLGA nanoparticles (NP1, NP2, NP3, NP4 in Table 1) to assess their physicochemical properties *in vitro*. The average particle size of the PLGA nanoparticles with a hydrophilic mPEG surface (NP1, NP2, NP4) was approximately 160 nm, similar to that of NP1 nanoparticles shown in Fig. 2a. However, NP3 nanoparticles without mPEG did not prevent extensive particular aggregation due to a hydrophobic interaction of the PLGA surface, resulting in the formation of larger particles (~2 μm in diameter). Except for the NP3 nanoparticles, PLGA nanoparticles (NP1, NP2, NP4) were stable for one month under optimal conditions without any precipitation. Over this time, no changes in the size of the nanoparticles were observed (data not shown). The image obtained from FE-SEM revealed that PLGA nanoparticles are almost spherical (Fig. 2b). Their zeta potentials ranged from −4.1 mV to −3.3 mV (Fig. 2c), indicating that their negative zeta potentials originated from PLGA, mPEG, Ce6 (Oh et al., 2012; Guo and Gemeinhart, 2008; Park et al., 2012), and were not significantly different. It is known that the zeta potential of colloidal particles strongly influences their stability and half-life in blood (Lee et al., 2010; Socha et al., 2009). A lower zeta potential generally increases the colloidal stability and the circulation period in the body (Lee et al., 2010; Socha et al., 2009). Furthermore, PEGylation to particles have enabled to decrease the uptake of particles by the reticular endothelial system (RES) in the liver and the spleen or immune cells, such as macrophages (Lee et al., 2008, 2010). Our PEGylated PLGA nanoparticles will present a prologed circulation time in body. To substantiate this potential, further *in vivo* investigations such as pharmacokinetic test will be required.

In addition, Fig. 2d shows the spherical shape of PLGA nanoparticles and the homogenous distribution of Ce6 in PLGA nanoparticles, confirmed by the Ce6 fluorescent image obtained from a fluorescence microscope.

3.2. Phototoxicity of PLGA nanoparticles

Fig. 3a presents the singlet oxygen generation from PLGA nanoparticles during light illumination. For this test, we utilized 9,10-dimethylanthracene (DMA) as an extremely fast chemical trap for the singlet oxygen (Park et al., 2011, 2012; Oh et al., 2012). Fluorescent DMA reacts selectively with the singlet oxygen to generate endoperoxide (Gomes et al., 2005), thus causing the reduction in the fluorescence of DMA. We illuminated PLGA nanoparticles with Ce6 molecules (NP1, NP2, NP3, equivalent Ce6 10 μg/mL) or free Ce6 (10 μg/mL) for 10 min at a light intensity of 5.2 mW/cm^2 using a 670 nm laser source. Changes in DMA fluorescence intensity were monitored in order to confirm singlet oxygen generation from PLGA nanoparticles or free Ce6. The change in the DMA fluorescence intensity (F_f–F_s) indicates the generation of substantially more singlet oxygen (Park et al., 2011, 2012; Oh et al., 2012). PLGA nanoparticles (NP1, NP2) stabilized in PBS (150 mM, pH 7.4) generated higher singlet oxygen than free Ce6 partially aggregated (Park et al., 2011, 2012) in PBS. Furthermore, the NP3 nanoparticles (~2 μm in diameter) aggregated in PBS (150 mM, pH 7.4) appeared to be self-quenched (Park et al., 2011, 2012), causing a significant reduction of singlet oxygen generation from Ce6 during light illumination. The enhanced singlet oxygen generation of NP1 nanoparticles allowed relatively higher phototoxicity for human nasopharyngeal epidermal carcinoma KB cells (Fig. 3b), considering that NP1 nanoparticles before light illumination has no cytotoxicity for up to 1000 μg/mL in 24 h of culture (Fig. 3c). In addition, the phototoxicities of NP1 and NP2 nanoparticles were not different (data not shown).

3.3. In vivo imaging and photodynamic therapy of PLGA nanoparticles

Fig. 4 shows an impressive contrast in *in vivo* fluorescent intensities between the samples. Photo-sensitizing properties of the Ce6 molecule in a near-infrared (NIR) region have been frequently utilized to obtain a light-driven fluorescent *in vivo* image in animals (Park et al., 2011, 2012; Oh et al., 2012; Baik et al., 2011). The NP1 nanoparticles (equivalent Ce6 0.1 mg/kg body) administered intravenously into KB tumor-bearing nude mice resulted in a strong fluorescent Ce6 signal in the tumor site and provided a clearer image of the tumor, although a fluorescent intensity was also noted in the liver and the kidney. This result is comparable to that administered free Ce6 (2.5 mg/kg) was localized in the kidney. In particular, despite the high-dose administration of free Ce6 (up to 2.5 mg/kg body), free Ce6 demonstrated a very weak fluorescent Ce6 signal in the tumor site, reflecting its inefficiency for tumor targeting. It seems that the enhanced permeability and retention

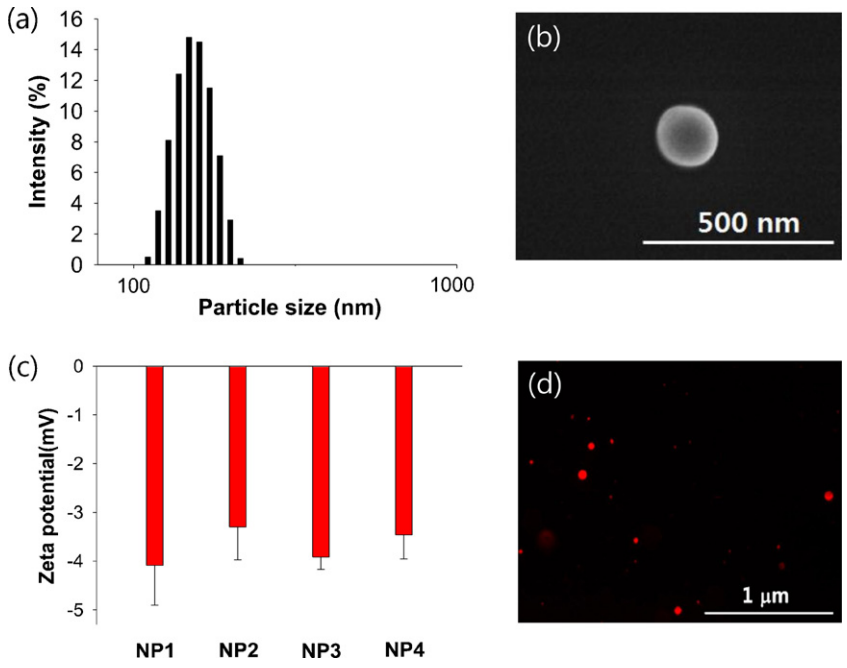

Fig. 2. Characterization of PLGA nanoparticles. (a) Particle size distribution of PLGA nanoparticle (NP1). (b) FE-SEM images of NP1. (c) Zeta-potential of PLGA nanoparticles. The concentration of each solution (PBS 150 mM, pH 7.4) was 0.1 mg/mL ($n = 3$). (d) Fluorescence image of NP1 (red fluorescence: Ce6). (For interpretation of the references to color in this figure legend, the reader is referred to the web version of the article.)

(EPR) effect (Maeda and Matsumura, 2011) caused the extravasation of NP1 nanoparticles from the tumor vasculature and led to preferential accumulation of NP1 nanoparticles in tumor tissues *in vivo*. This behavior of NP1 nanoparticles was also similar to that seen with fluorescent *in vivo* image of KB tumor-bearing nude mice treated with NP2 nanoparticles (data not shown).

Fig. 5a shows *in vivo* T_2^*-weighted MR imaging of each sample for KB tumor-bearing nude mice. The NP1 nanoparticles employing Fe_3O_4 (*i.v.* dose: equivalent Fe 0.5 mg/kg) displayed an enhanced T_2^* negative MR image for the tumor compared to the commercially available Feridex® (*i.v.* dose: Fe 5 mg/kg). The NP1 nanoparticles accumulating at tumor sites may diminish the spin–spin

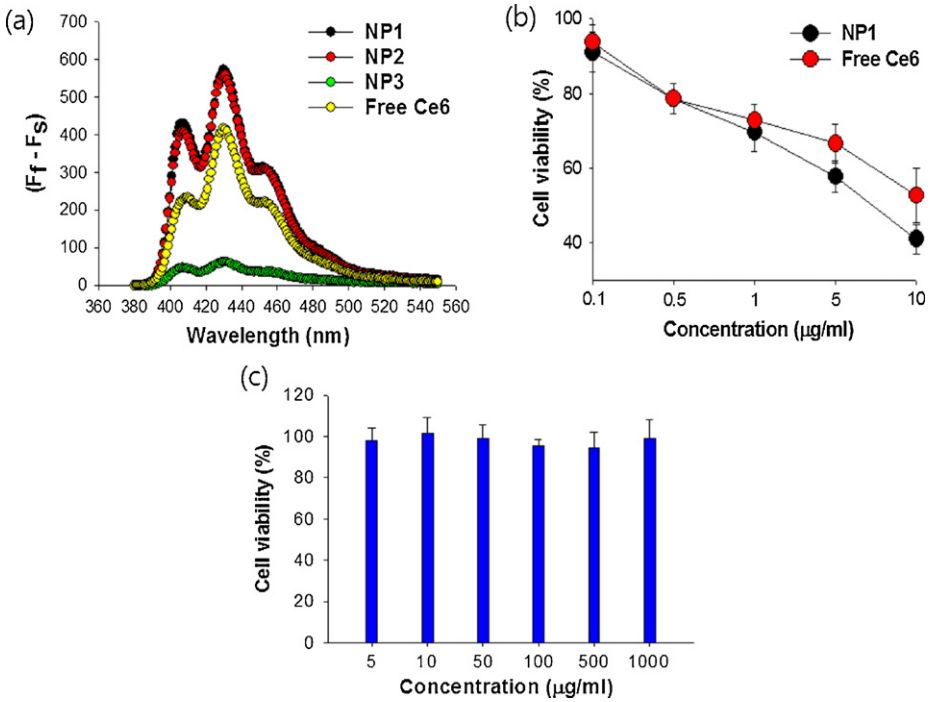

Fig. 3. Light-sensitive properties of PLGA nanoparticles *in vitro*. (a) The 9,10-dimethylanthracene fluorescence change (at λ_{ex} 360 nm and λ_{em} 380–550 nm) of each PLGA nanoparticle or free Ce6 in PBS (150 mM, pH 7.4). Singlet oxygen generation is indicated by change in the 9,10-dimethylanthracene fluorescence intensity (F_f–F_s, where F_f is the full 9,10-dimethylanthracene fluorescent intensity and F_s is the fluorescence intensity of each sample). (b) Phototoxicities determined by a Cell Counting Kit-8 (CCK-8) of KB cells treated with NP1 or free Ce6. All cells were irradiated for 10 min at a light intensity of 5.2 mW/cm^2 using a 670 nm laser source and were then incubated for an additional 12 h ($n = 7$). (c) Cell viabilities of KB cells treated with NP1 (5–1000 μg/mL) without light illumination for 24 h ($n = 8$).

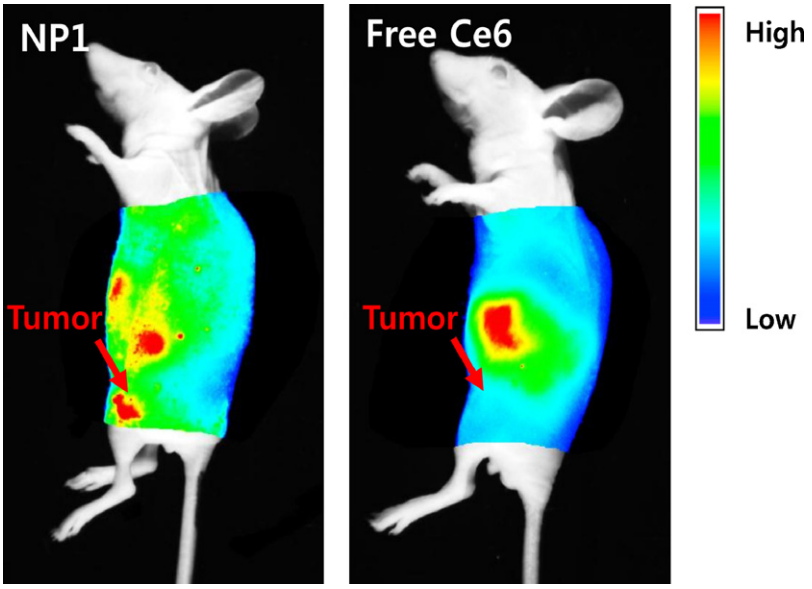

Fig. 4. *In vivo* non-invasive fluorescent imaging of nude mice harboring KB tumors. NP1 (*i.v.* dose: equivalent Ce6 0.1 mg/kg) or free Ce6 (*i.v.* dose: 2.5 mg/kg) was intravenously injected into KB tumor-bearing nude mice through the tail vein, and fluorescent images were obtained after 8 h.

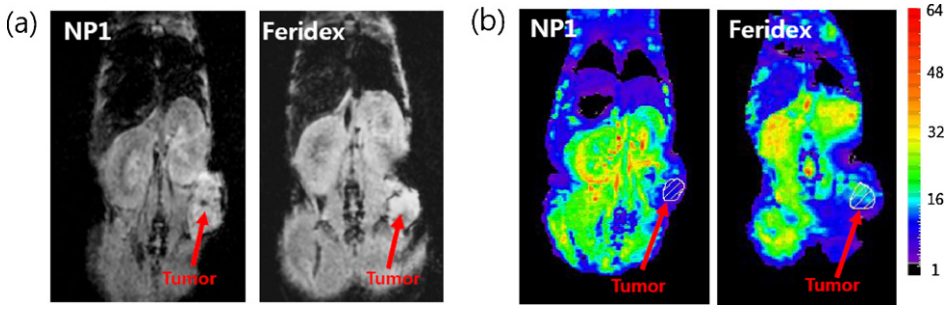

Fig. 5. (a) *In vivo* T_2^*-weighted MR imaging. NP1 (*i.v.* dose: equivalent Fe 0.5 mg/kg) or Feridex® (*i.v.* dose: Fe 5 mg/kg) was intravenously injected into KB tumor-bearing nude mice through the tail vein. (b) Color mapping of the identical T_2^*-weighted MR images.

relaxation time (T_2^*) by dephasing the spin of neighboring water protons (Fortnum et al., 2009), leading to the darkening of T_2^*-weighted image in the tumor site (Fig. 5). Color mapping for the darkness of identical T_2^*-weighted MR images (Fig. 5b) shows more details of MR signal changes. Improved T_2^* negative image of NP1 nanoparticles indicates that NP1 nanoparticles can be utilized as a novel MR imaging agent with a light luminescence activity.

Fig. 6 shows the tumor volume regression of KB tumor-bearing nude mice injected only once with NP1 nanoparticles (equivalent Ce6 0.1 mg/kg body) or free Ce6 (2.5 mg/kg). At 24 h

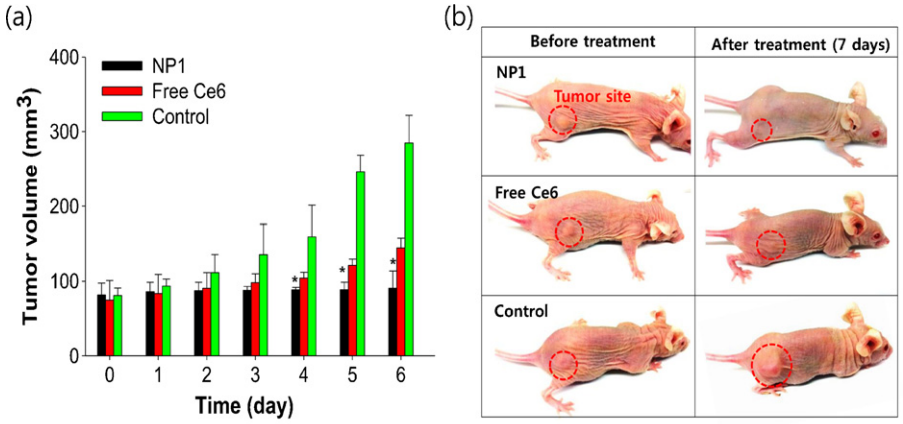

Fig. 6. *In vivo* anti-tumor effect by PLGA nanoparticles. (a) Tumor volume regression in KB tumor-bearing nude mice injected with illuminated NP1 (*i.v.* dose: equivalent Ce6 0.1 mg/kg body), free Ce6 (*i.v.* dose: 2.5 mg/kg) or only PBS (150 mM) (control) (illumination for 40 min at a light intensity of 5.2 mW/cm^2 using a 670 nm laser source) ($n = 5$). (b) Optical photographs of KB tumor-bearing nude mice. The tumor site is indicated by a red dotted line. (For interpretation of the references to color in this figure legend, the reader is referred to the web version of the article.)

post-injection, tumor sites were locally illuminated at a light intensity of 5.2 mW/cm^2 using a 670 nm laser source for 40 min. The administration of NP1 nanoparticles resulted in a significant growth inhibition of the KB tumors. The tumor volume in the nude mice treated with NP1 nanoparticles was approximately 1.5 or 3 times smaller than those treated with free Ce6 or PBS (control). When compared to high-dose administration of free Ce6 (2.5 mg/kg), low-dose administration of NP1 nanoparticles (equivalent Ce6 0.5 mg/kg body) were found to be more efficient for tumor regression.

4. Conclusion

Multifunctional PLGA nanoparticles exhibited an improved *in vivo* luminescence imaging and photodynamic therapy for the tumor site. The encapsulation of Fe_3O_4 allowed high contrast MRI *in vivo* tumor imaging. Overall, the collective results from a series of both *in vivo* imaging and therapy studies strongly support that multifunctional PLGA nanoparticles can improve effective tumor diagnosis and treatment. We expect that these PLGA nanoparticles that can be tailor-made for the desired functionality can further advance the technology for efficient anti-tumor management.

Acknowledgement

This work was financially supported by a grant of the Korean Health Technology R&D Project, Ministry of Health & Welfare (No. A111291), Republic of Korea.

References

Alivisatos, P., 2003. The use of nanocrystals in biological detection. Nat. Biotechnol. 22, 47–52.
Bagalkot, V., Zhang, L., Levy-Nissenbaum, E., Jon, S., Kantoff, P.W., Langer, R., Farokhzad, O.C., 2007. Quantum dot-aptamer conjugates for synchronous cancer imaging, therapy, and sensing of drug delivery based on bi-fluorescence resonance energy transfer. Nano Lett. 7, 3065–3070.
Baik, H.J., Oh, N.M., Oh, Y.T., Yoo, N.Y., Park, S.Y., Oh, K.T., Youn, Y.S., Lee, E.S., 2011. 3-Diethylaminopropyl-bearing glycol chitosan as a protein drug carrier. Colloids Surf. B: Biointerfaces 84, 585–590.
Brannon-Peppas, L., Blanchette, J.O., 2004. Nanoparticle and targeted systems for cancer therapy. Adv. Drug Deliv. Rev. 56, 1649–1659.
Chin, W.W.L., Lau, W.K.O., Heng, P.W.S., Bhuvaneswari, R., Olivo, M., 2006. Fluorescence imaging and phototoxicity effects of new formulation of chlorin e6-polyvinylpyrrolidone. J. Photochem. Photobiol. B: Biol. 84, 103–110.
Ferrari, M., 2005. Cancer nanotechnology: opportunities and challenges. Nat. Rev. Cancer 5, 161–171.
Fortnum, H., O'Neil, C., Taylor, R., Lenthall, R., Nikolopoulos, T., Lightfoot, G., O'Donoghue, G., Mason, S., Baguley, D., Jones, H., Mulvaney, C., 2009. The role of magnetic resonance imaging in the identification of suspected acoustic neuroma: a system review of clinical and cost effectiveness and natural history. Health Technol. Assess. 13, 1–154.
Gomes, A., Fernandes, E., Lima, J.L.F.C., 2005. Fluorescence probes used for detection of reactive oxygen species. J. Biochem. Biophys. Methods 65, 45–80.
Guo, C., Gemeinhart, R.A., 2008. Understanding the adsorption mechanism of chitosan onto poly(lactide-co-glycolide) particles. Eur. J. Pharm. Biopharm. 70, 597–604.
Hamblin, M.R., Miller, J.L., Rizvi, I., Ortel, B., Maytin, E.V., Hasan, T., 2001. Pegylation of a chlorine6 polymer conjugate increases tumor targeting of photosensitizer. Cancer Res. 61, 7155–7162.
Kim, J., Lee, J.E., Lee, S.H., Yu, J.H., Lee, J.H., Park, T.G., Hyeon, T., 2008. Designed fabrication of a multifunctional polymer nanomedical platform for simultaneous cancer-targeted imaging and magnetically guided drug delivery. Adv. Mater. 20, 478–483.
Kizilel, S., Scavone, A., Liu, X., Nothias, J.M., Ostrega, D., Witkowski, P., Millis, M., 2010. Encapsulation of pancreatic islets within nano-thin functional polyethylene glycol coatings for enhanced insulin secretion. Tissue Eng. A 16, 2217–2228.
Lee, B.R., Oh, K.T., Oh, Y.T., Baik, H.J., Park, S.Y., Youn, Y.S., Lee, E.S., 2011a. A novel pH-responsive polysaccharidic ionic complex for proapoptotic D-(KLAKLAK) 2 peptide delivery. Chem. Commun. 47, 3852–3854.
Lee, E.S., Gao, Z., Bae, Y.H., 2008. Recent progress in tumor pH targeting nanotechnology. J. Control. Release 132, 164–170.
Lee, E.S., Park, K.H., Kang, D., Park, I.S., Min, H.Y., Lee, D.H., Kim, S., Kim, J.H., Na, K., 2007. Protein complexed with chondroitin sulfate in poly (lactide-*co*-glycolide) microspheres. Biomaterials 28, 2754–2762.
Lee, H.J., Kim, S.E., Kwon, I.K., Park, C., Kim, C., Yang, J., Lee, S.C., 2010. Spatially mineralized self-assembled polymeric nanocarriers with enhanced robustness and controlled drug-releasing property. Chem. Commun. 46, 377–379.
Lee, S.J., Jeong, J.R., Shin, S.C., Kim, J.C., Chang, Y.H., Chang, Y.M., Kim, J.D., 2004. Nanoparticles of magnetic ferric oxides encapsulated with poly (D,L latide-co-glycolide) and their applications to magnetic resonance imaging contrast agent. J. Magn. Magn. Mater. 272, 2432–2433.
Lee, W.R., Oh, K.T., Park, S.Y., Yoo, N.Y., Ahn, Y.S., Lee, D.H., Youn, Y.S., Lee, D.K., Cha, K.H., Lee, E.S., 2011b. Magnetic levitating polymeric nano/microparticular substrates for three-dimensional tumor cell culture. Colloids Surf. B: Biointerfaces, 379–384.
Liong, M., Lu, J., Kovochich, M., Xia, T., Ruehm, S.G., Nel, A.E., Tamanoi, F., Zink, J.I., 2008. Multifunctional inorganic nanoparticles for imaging, targeting, and drug delivery. ACS Nano 2, 889–896.
Maeda, H., Matsumura, Y., 2011. EPR effect based drug design and clinical outlook for enhanced cancer chemotherapy. Adv. Drug Deliv. Rev. 63, 129–130.
Neises, B., Steglich, W., 1978. Simple method for the esterification of carboxylic acids. Angew. Chem. Int. Ed. Engl. 17, 522–524.
Niemeyer, C.M., 2001. Nanoparticles, proteins, and nucleic acids: biotechnology meets materials science. Angew. Chem. Int. Ed. Engl. 40, 4128–4158.
Ochsner, M., 1997. Photophysical and photobiological processes in the photodynamic therapy of tumours. J. Photochem. Photobiol. B: Biol. 39, 1–18.
Oh, N.M., Kwag, D.S., Oh, K.T., Youn, Y.S., Lee, E.S., 2012. Electrostatic charge conversion processes in engineered tumor-identifying polypeptides for targeted chemotherapy. Biomaterials 33, 1884–1893.
Park, S.Y., Baik, H.J., Oh, Y.T., Oh, K.T., Youn, Y.S., Lee, E.S., 2011. A smart polysaccharide/drug conjugate for photodynamic therapy. Angew. Chem. Int. Ed. Engl. 50, 1644–1647.
Park, S.Y., Oh, K.T., Oh, Y.T., Oh, N.M., Youn, Y.S., Lee, E.S., 2012. An artificial photosensitizer drug network for mitochondria-selective photodynamic therapy. Chem. Commun. 48, 2522–2524.
Peer, D., Karp, J.M., Hong, S., Farokhzad, O.C., Margalit, R., Langer, R., 2007. Nanocarriers as an emerging platform for cancer therapy. Nat. Nanotechnol. 2, 751–760.
Piao, Y., Kim, J., Na, H.B., Kim, D., Baek, J.S., Ko, M.K., Lee, J.H., Shokouhimehr, M., Hyeon, T., 2008. Wrap–bake–peel process for nanostructural transformation from β-FeOOH nanorods to biocompatible iron oxide nanocapsules. Nat. Mater. 7, 242–247.
Prashant, C., Dipak, M., Yang, C.T., Chuang, K.H., Jun, D., Feng, S.S., 2010. Superparamagnetic iron oxide – loaded poly (lactic acid)-d-α-tocopherol polyethylene glycol 1000 succinate copolymer nanoparticles as MRI contrast agent. Biomaterials 31, 5588–5597.
Qian, X., Peng, X.H., Ansari, D.O., Yin-Goen, Q., Chen, G.Z., Shin, D.M., Yang, L., Young, A.N., Wang, M.D., Nie, S., 2008. In vivo tumor targeting and spectroscopic detection with surface-enhanced Raman nanoparticle tags. Nat. Biotechnol. 26, 83–90.
Reddy, G.R., Bhojani, M.S., McConville, P., Moody, J., Moffat, B.A., Hall, D.E., Kim, G., Koo, Y.E.L., Woolliscroft, M.J., Sugai, J.V., 2006. Vascular targeted nanoparticles for imaging and treatment of brain tumors. Clin. Cancer Res. 12, 6677–6686.
Socha, M., Bartecki, P., Passirani, C., Sapin, A., Damge, C., Lecompte, T., Barre, J., EI Ghazouani, F., Maincent, P., 2009. Stealth nanoparticles coated with heparin as peptide or protein carriers. J. Drug Target. 17, 575–585.
Takizawa, H., Kondo, K., Toba, H., Kenzaki, K., Sakiyama, S., Tangoku, A., 2009. Fluorescence diagnosis of lymph node metastasis of lung cancer in a mouse model. Oncol. Rep. 22, 17–21.
Zhang, N., Chittasupho, C., Duangrat, C., Siahaan, T.J., Berkland, C., 2007. PLGA nanoparticle-peptide conjugate effectively targets intercellular cell-adhesion molecule-1. Bioconjug. Chem. 19, 145–152.